Sensors and Actuators B 260 (2018) 617–626

Contents lists available at ScienceDirect

Sensors and Actuators B: Chemical

journal homepage: www.elsevier.com/locate/snb

Development of molecular imprinted sol-gel based LSPR sensor for detection of volatile *cis*-jasmone in plant

Liang Shang [a], Chuanjun Liu [a,b], Bin Chen [c], Kenshi Hayashi [a,*]

[a] Department of Electronics, Graduate School of Information Science and Electrical Engineering, Kyushu University, Fukuoka, 819-0395, Japan
[b] Research Laboratory, U.S.E. Co., Ltd., Tokyo, 150-0013, Japan
[c] College of Electronic and Information Engineering, Southwest University, Chongqing, 400715, China

ARTICLE INFO

Article history:
Received 21 July 2017
Received in revised form
19 December 2017
Accepted 19 December 2017
Available online 28 December 2017

Keywords:
Plant volatile organic compounds
cis-Jasmone
Localized surface plasma resonance
Molecularly imprinted sol-gel
Functional monomer
Optical sensor

ABSTRACT

Detection of *cis*-jasmone (CJ) enables monitoring of growth pressure in plants, which is especially useful for sensing attacks by herbivores. Here, a sensitive and selective nanocomposite-imprinted, localized surface plasmon resonance (LSPR) sensor for CJ vapor was fabricated. Gold (Au) nano-islands were prepared by vacuum sputtering of Au nanoparticles on a glass substrate, followed by thermal annealing. Titanium molecularly imprinted sol-gels (MISGs) were spin-coated on the Au nano-islands as an adsorption layer for enhancing the selectivity of the optical sensor. Gas molecules were detected by using a small spectrometer to monitor variations in absorption spectra. In addition, the functional monomer and the ratio of matrix materials to functional monomers in the MISGs were investigated and optimized. MISGs that contained the functional monomer trimethoxyphenylsilane at a 3:1(v:v) ratio exhibited a higher sensitivity and selectivity than other films. The optical sensor would have advantages of low cost, selectivity, sensitivity, and repeatability. The limit of CJ detection in air was 3.5 ppm (signal/noise = 3). Thus, the sensor is expected to be a potential tool for CJ monitoring in agriculture applications.

1. Introduction

Plants have evolved a variety of sophisticated mechanisms to withstand stresses imposed by salt, cold, heat, herbivore attack, or pathogen infection [1]. A critical mechanism for self-protection, as well as a communication signal between plants, is the production of complex mixtures of plant volatile organic compounds (PVOCs) [2]. PVOCs can not only attract pollinators or seed-dispersing animals, but also repel potential herbivores [3]. Recently, much effort has been focused on clarifying the metabolic pathways and functions of these PVOCs [4,5]. Sobhy et al. suggested that (*E*)-2-hexenal, methyl salicylate, *cis*-jasmone (CJ), and methyl benzoate were the main compounds in the PVOCs [6]. In particular, jasmone released by flowers or leaves can be used as a chemical cue for herbivorous insect infestation [7]. In addition, Birkett et al. reported that the biosynthesis of CJ was associated with stress-induced jasmonic acid or octadecanoid pathways [8–10]. Bruce et al. reported that CJ treatment of crop plants, such as soybeans and potatoes, directly defended against aphids, and also initiated PVOC release that repelled natural enemies [11]. Therefore, CJ can be regarded as a vital biomarker for plant pest and disease monitoring in agriculture [12]. Currently, PVOCs has been analyzed with gas chromatography/mass [13]. However, this is not suitable for real-time PVOC monitoring because it is time consuming, costly, and not portable. [14,15]. Therefore, alternative sensing strategies need to be considered for real-time monitoring of CJ vapors with high sensitivity, selectivity, and response speeds for agricultural applications [16].

Recently, plasmonic signal transduction has been used to enhance the sensitivity of biosensor probes and chemical sensors [17–19]. Localized surface plasmon resonance (LSPR) involves the interaction of metallic nanoparticles (NPs) with electromagnetic waves to induce plasmon oscillations at NP surfaces [20–22]. LSPR can be used as a transducer by converting changes in refractive index (RI) into spectral shifts through induced electromagnetic fields [23,24]. Because of its rapid response and high sensitivity, LSPR has led to the development of optical sensors for various analytes, such as polyphosphates, blood plasma, and wine [25–29].

Because responses of LSPR sensors depend on changes in the media surrounding the NPs, there is a low selectivity for target analytes [30,31]. Therefore, absorbing materials or antibodies are always coated on the NP surfaces to enhance sensitivity and selectivity [32,33]. In our previous work, LSPR sensors coated

* Corresponding author.
E-mail addresses: shang.liang.100@s.kyushu-u.ac.jp (L. Shang), liu@o.ed.kyushu-u.ac.jp (C. Liu), chenbin121@swu.edu.cn (B. Chen), hayashi@ed.kyushu-u.ac.jp (K. Hayashi).

https://doi.org/10.1016/j.snb.2017.12.123
0925-4005/

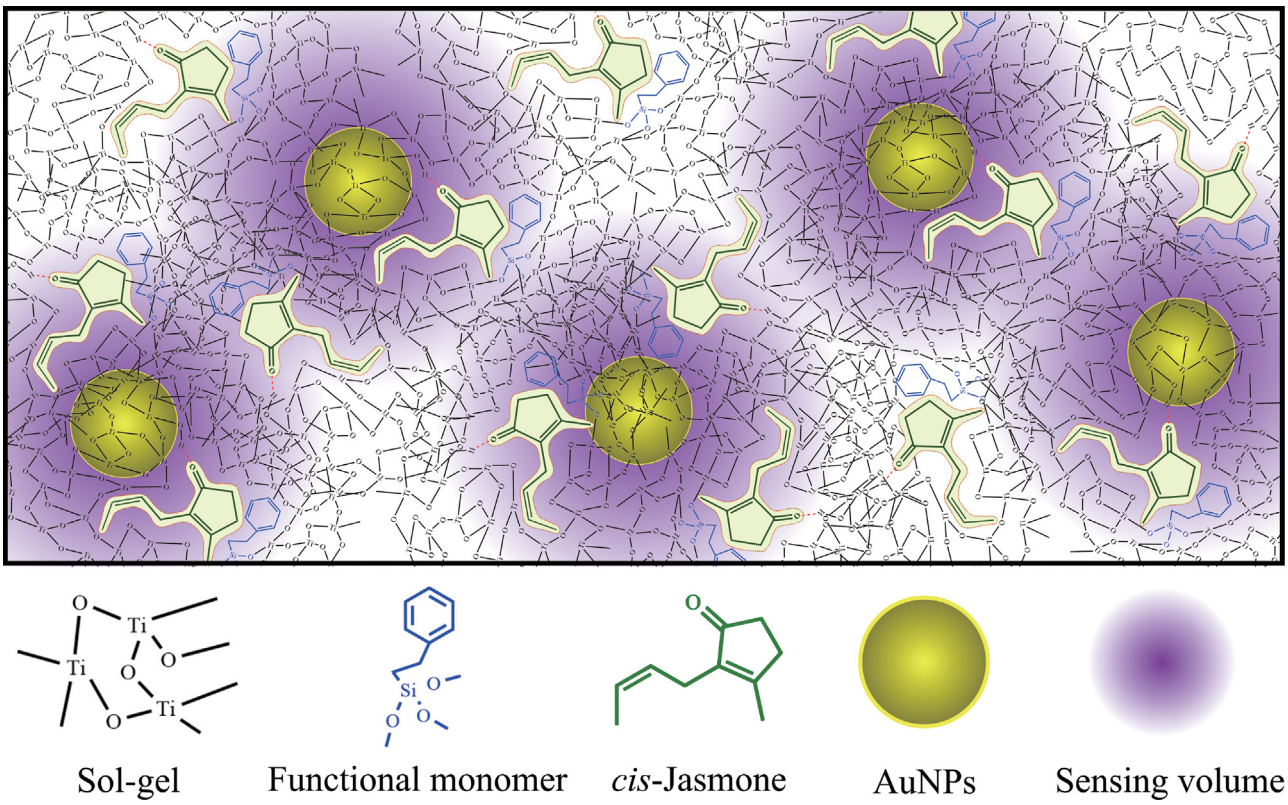

Fig. 1. Schematic of MISG-coated Au nano-islands with functional monomers for selective CJ vapor detection.

with molecularly imprinted polymers (MIPs) were developed for terpene vapor detection [34]. Molecular imprinting involves molecular recognition with high selectivity to target molecules [35,36]. By controlling the thickness of MIP layers and the NP structure, both high sensitivity and selectivity can be balanced very well. However, organic polymers have some limitations, such as poor site accessibility and chemical stability [37]. Molecularly imprinted sol-gels (MISGs) have high selectivity, low cost, long life cycles, and tailored physical-chemical properties [38]. Thus, MISGs have been used for chromatographic separations and chemical sensors [39].

The aim of this work was to develop a MISG-based LSPR for detection of CJ. As illustrated in Fig. 1, Au nano-islands were fabricated by vacuum sputtering and annealing. Then, a three dimensional "imprint" of CJ molecules within the MISG was created around the Au nano-islands. An optical sensor was developed for CJ detection by monitoring changes in the RI by absorbance spectra. The functional monomer was a vital element of the MISGs, and was investigated to enhance imprinting effects for sensitivity. In addition, the effect of the ratio of matrix material to functional monomer on the CJ response was examined. The feasibility of the MISG-LSPR sensor for CJ vapor was evaluated.

2. Materials and methods

2.1. Materials and instrumentations

Tetrabutoxy titanium (TBOT), isopropanol, CJ, limonene, γ-terpene, titanium tetrachloride ($TiCl_4$), acetone, and ethanol were purchased from Wako Pure Chemical Industries, Japan. 3-aminopropyl tri-ethoxysilane (APTES) was purchased from Shin-Etsu Chemical, Japan. α-pinene, trimethoxyphenylsilane (TMP), triethoxy phenylsilane (TEP), trimethoxy(2-phenylethyl)silane (TM2P) were purchased from Sigma-Aldrich Co. LLC, USA. Benzyltriethoxysilane (BTE) was purchased from Tokyo Chemical Industry Co., Japan. All reagents were used as received. Fourier transform-infrared spectroscopy (FT-IR, Nicolet iS 5, Thermo Fisher Scientific, USA) was used to analyze MISG-AuNP films before and after CJ absorption. Scanning electron microscopy (SEM, SU8000, Hitachi) and atomic force microscopy (AFM, Dimension Ion, Bruker IXS) were used to image morphologies of AuNP-coated NISGs/MISGs.

2.2. Preparation of MISG reaction solution

Preparation of the MISG reaction solution was reported previously [40]. Briefly, it was prepared by dissolving 0.441 mmol (150 μL) TBOT precursor, 0.304 mmol (50 μL) CJ templates, and 50 μL of functional monomers (TMP, TEP, TM2P, or BTE) in 2 mL of isopropanol while stirring. The concentrations of TMP, TEP, TM2P, or BTE in the MISG solutions were 0.252 mmol, 0.208 mmol, 0.221 mmol, and 0.197 mmol, respectively (see Fig. 2 for structures). Then, 0.132 mmol (25 μL) of $TiCl_4$ was added to initiate the reaction. Afterward, the MISG reaction solution was pre-hydrolyzed in a 60 °C water bath for 1 h while stirring. Finally, the solution was stirred at room temperature (25 °C) for 8 h to compete the MISG reaction.

2.3. MISG-coated LSPR sensor preparation

A 12-mm × 9-mm glass substrate was ultrasonically cleaned in ultrapure water, acetone, ethanol, and then exposed to an argon plasma (PDC-001, Harrick plasma, USA). It was then immersed in a 1:10 (v:v) APTES ethanol solution for 8 h. After being cleaned with ethanol and dried with flowing nitrogen, the sample was put into a quick coater (SC-701 HMCII, Sanyu electron, Japan) for a 3-nm deposition of AuNP. Thermal annealing was then performed in a muffle furnace (SSTS–13 K, ISUZU, Seisakusho, Japan) at 500 °C for 2 h, followed by cooling to room temperature. The sample was then subjected to sputtering and annealing again under the same condi-

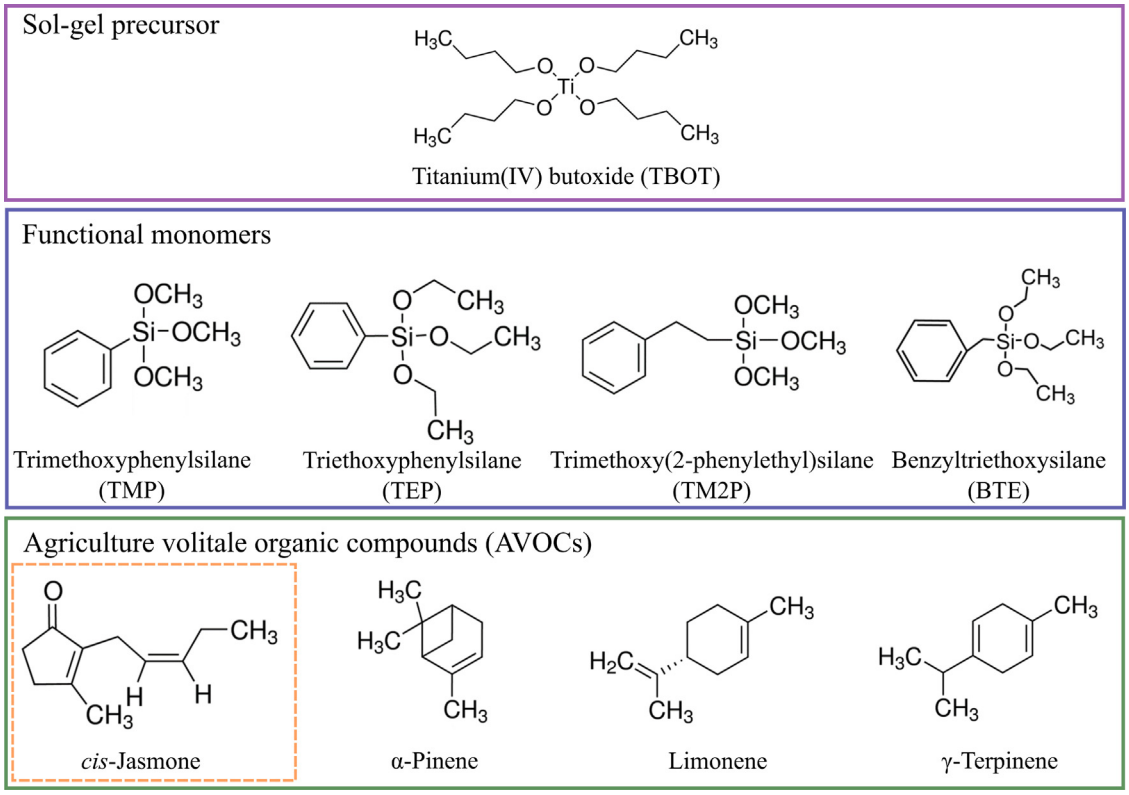

Fig. 2. Chemical structures of the matrix precursor, four functional monomers, and four types of PVOCs.

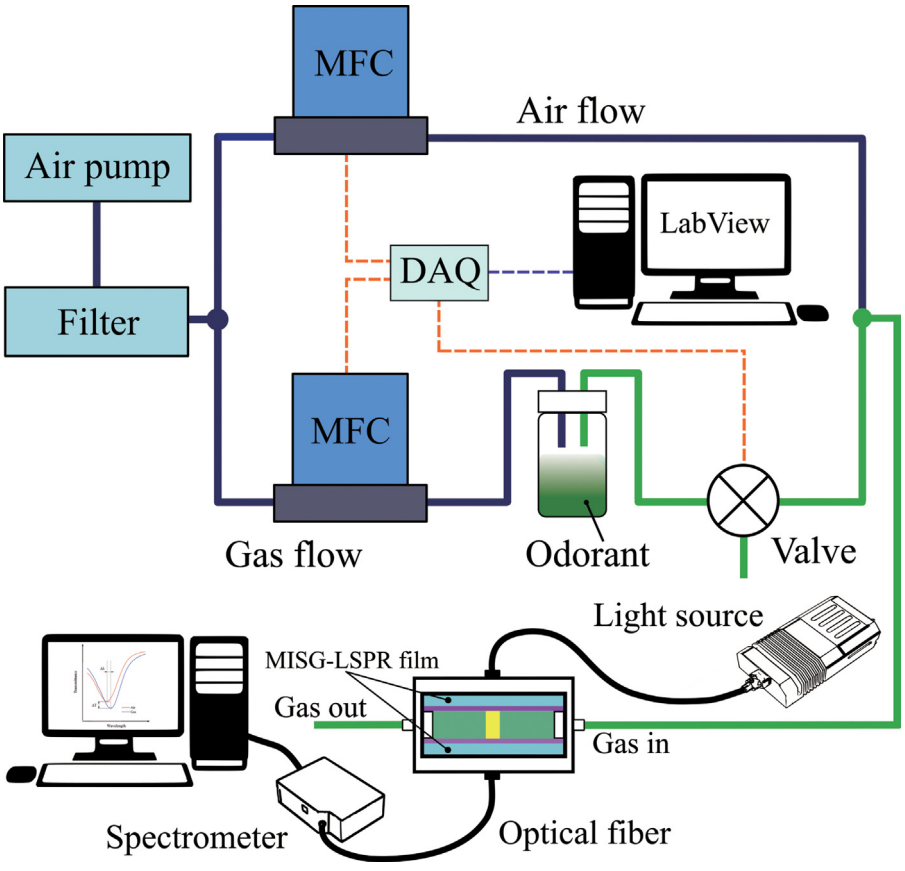

Fig. 3. Schematic of LSPR sensing platform and PVOC generation.

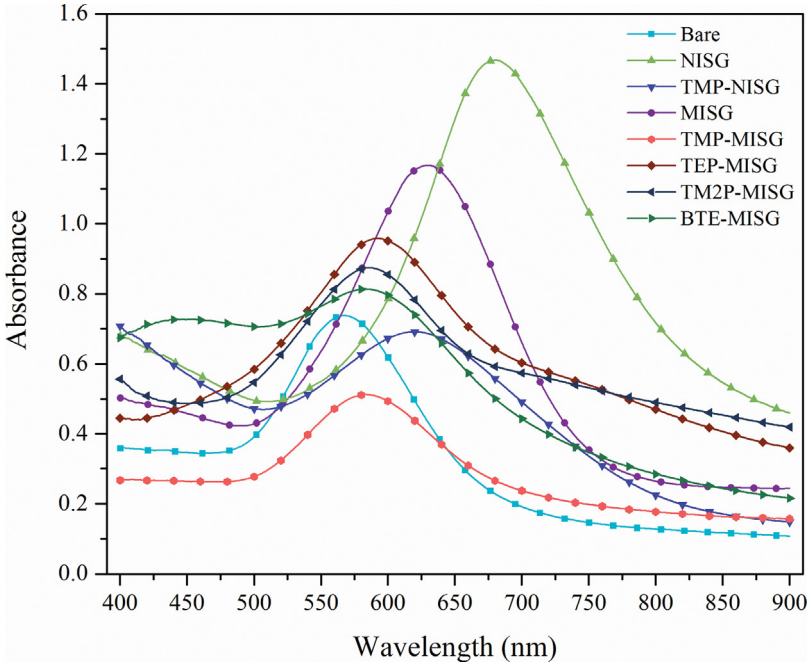

Fig. 4. Absorption spectra for the bare substrate, a NISGs coat, and MISGs coatings with different functional monomers.

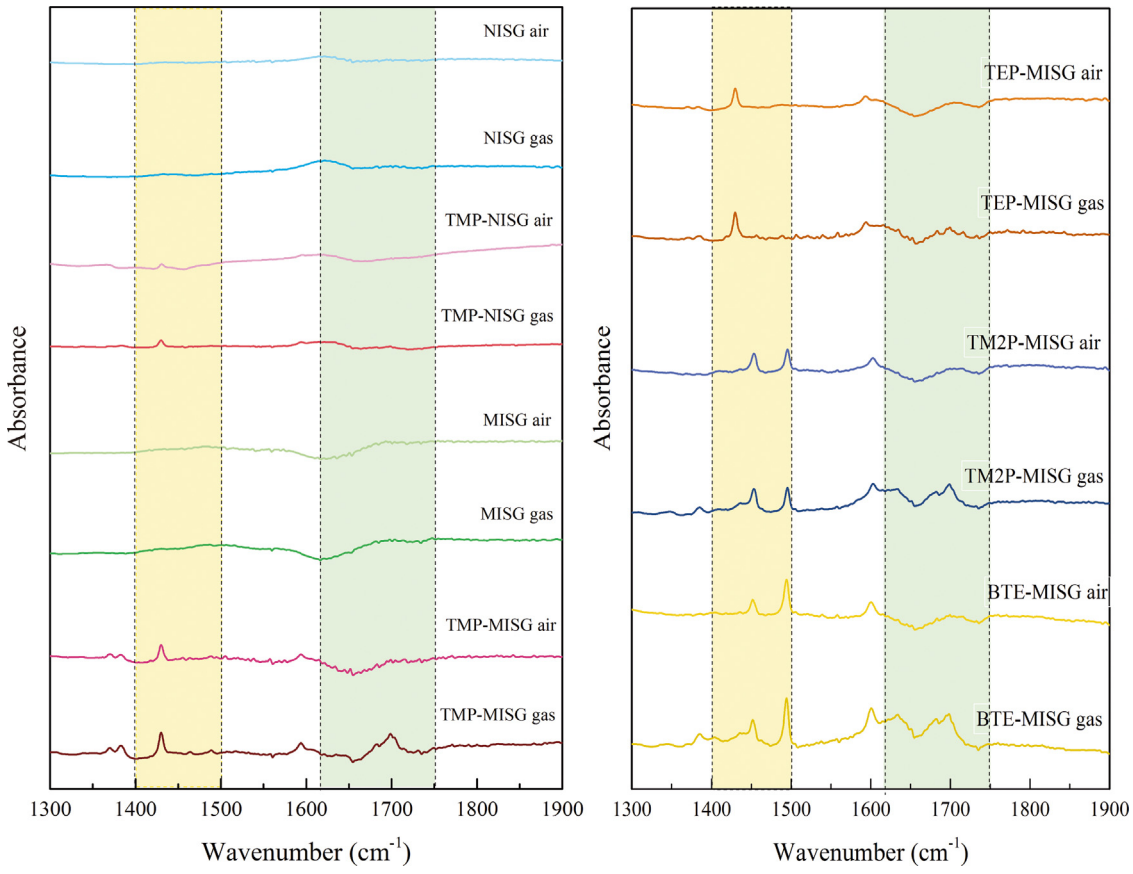

Fig. 5. FT-IR spectra of NISG-, TMP-NISG-, MISG-, TMP-MISG-, TEP-MISG-, TM2P-MISG-, and BTE-MISG-coated samples before and after CJ vapor absorption.

tions to form a high-sensitivity LSPR substrate [41]. Then, 20 μL of the MISG reaction solution was spin-coated on the Au nano-islands at 3000 rpm for 1 min. In the last step, the sample was kept at 130 °C for 1 h to finish the MISG fabrication and to evaporate the templates. All samples were stored under vacuum to remove volatile organic compounds in the MISGs.

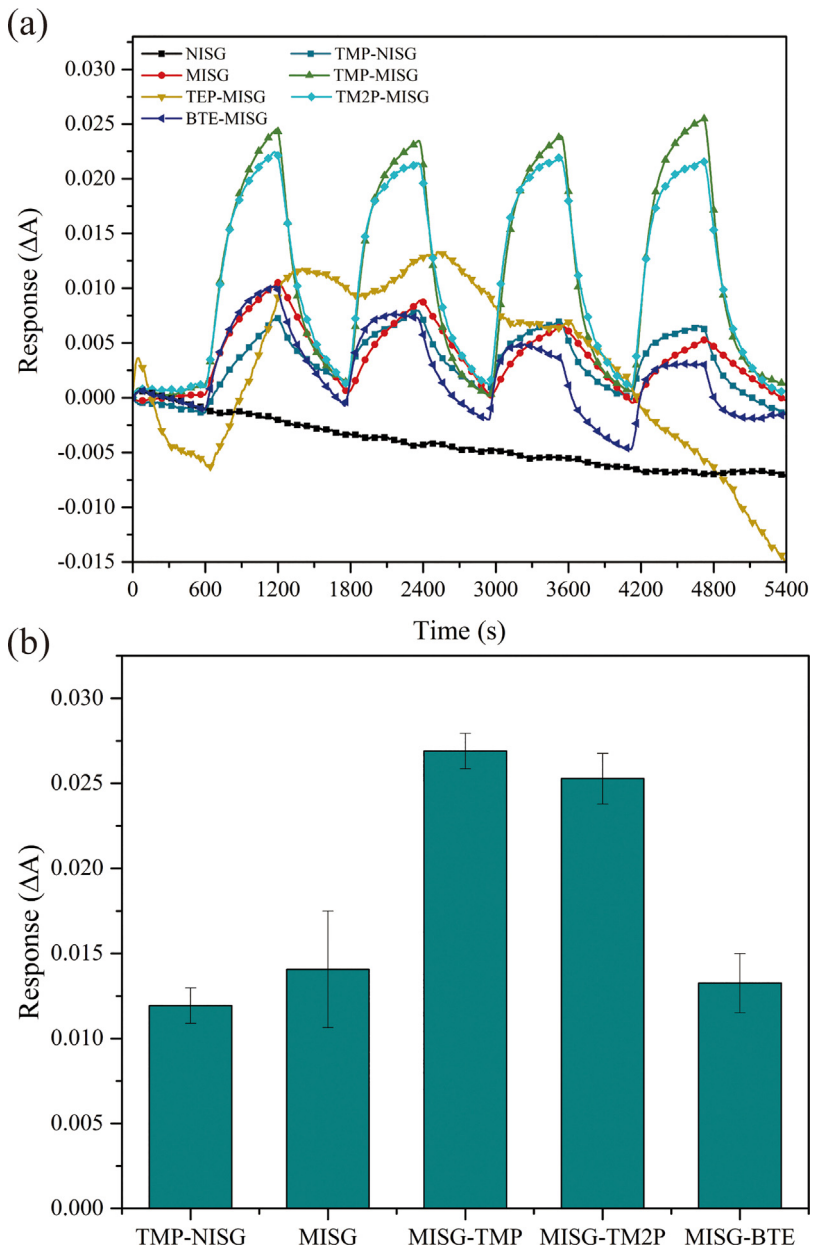

Fig. 6. Real-time responses for NISG-, MISG-, TMP-MISG-, TEP-MISG-, TM2P-MISG-, and BTE-MISG-coated samples (a) and their quantitative responses (b). Responses were obtained for a 600-s CJ vapor flow (10.56 ± 0.96 ppm), followed by a 600-s air flow.

2.4. Vapor generation and sensing system

Schematics of the PVOC vapor generation and optical sensing systems are shown in Fig. 3. Vapor was generated from a glass bottle with odorants (6 mL), and controlled with an air pump, a cleaning filter (filled with molecular sieves and activated carbon), two mass flow controllers (MFC), and a three-way valve. All gas flow paths used Teflon tubes. The gas/air flow was controlled with LabView software (2014, National instruments, Austin, USA) and a DAQ (USB-6009, National instruments, Austin, USA) card. The concentrations C (ppm) of PVOCs were calculated by:

$$C = \frac{k \times D_r \times 10^3}{F} \quad (1)$$

where D_r (μg/min) was the diffusion rate at the ambient temperature, F (L/min) was the flow rate of the diluent gas (0.5 L/min), and k was the factor for converting gas weight to gas volume, which was calculated by:

$$k = \frac{22.4}{M} \times \frac{273 + t}{273} \times \frac{760}{P} \quad (2)$$

M was the molecular weight of the PVOC molecule, t was the temperature of the gas chamber (25 °C), and P was the gas pressure (760 mmHg). By changing F and the size of the bottle, various concentrations of PVOCs could be obtained. The optical sensing system included a tungsten-halogen light source (LS-1, Ocean Optics, USA), a sensing cell, and an ultraviolet-visible (UV-vis) spectrometer (HR4000, Ocean Optics, USA). Absorption spectra were acquired over the range 400–900 nm at a resolution of 0.1 nm, and recorded by OPwave+ software (Ocean Optics, USA). Gas responses were obtained with a PVOC vapor flow for 600 s and then an air flow for 600 s.

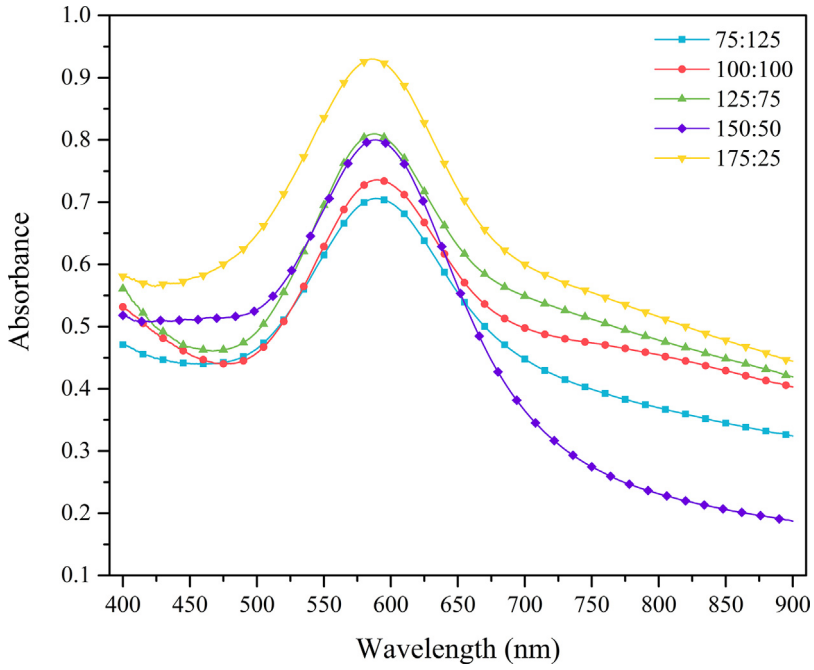

Fig. 7. Absorption spectra for TMP-MISG-coated samples with different TBOT/TMP ratios (v:v).

3. Results and discussion

3.1. Functional monomer selection

Strong noncovalent interactions between the functional monomers and the templates were critical for forming three-dimensional binding cavities during polymerization [42]. The functional monomer was a critical for MISGs preparation. CJ is very volatile, with a vapor pressure of 0.029 mm Hg at 25 °C. Therefore, it could be evaporated from the NISGs/MISGs layer with clean flowing air. Given the chemical structure of CJ (Fig. 2), functional monomers with aromatic rings would be appropriate for cavity generation in the MISGs via π – electron, Van der Waals, and hydrogen-bond interactions [43,44]. Therefore, four function monomers (TMP, TEP, TM2P and BTE) were considered (Fig. 2).

Au nano-islands coated with various MISGs were optically characterized. Fig. 4 plots differences in their UV–vis spectra. Relative to the bare sample, plasmon peaks in the NISG/MISG-coated samples shifted to the red because of the MISGs. In addition, relative to the MISG-modified sample, the surface plasmon (SP) peaks of the samples coated by MISG with functional monomers shifted to the blue. Their surface morphologies were imaged with SEM (Fig. S1) and AFM (Fig. S2). SEM of the bare sample revealed that Au nano-islands were uniformly deposited on the substrate, which would induce a stronger LSPR effect between Au nano-islands [45]. The islands were covered by MISG/NISG films, which produced the diverse absorbance spectra. The surfaces of MISG-coated samples varied with functional monomers, which indicated that the sol-gel process was affected differently by the functional monomers (TMP, TEP, TM2P, and BTE).

Attenuated total reflection FT-IR spectra were plotted in Fig. 5. The broadened band at 1400–1480 cm^{-1} was attributed to stretching of the benzenoid ring. There were benzenoid ring peaks in the functional monomers contained in the NISGs/MISGs; thus, the monomers were polymerized in the sol-gel films. The strong band at 1620–1750 cm^{-1} was attributed to C=O stretching of CJ, as was observed in the MISG-TMP- and MISG-TM2P-coated samples after gas absorption. Hence, CJ molecules diffused to the MISGs cavities (Fig. 2). In addition, lower-energy peaks appeared in the MISG- and MISG-BTE-coated samples. In contrast, there were no C=O absorption peaks in the NISG-modified samples, which indicated less gas absorption.

In-situ responses of NISG-, TMP-NISG-, MISG-, TMP-MISG-, TEP-MISG-, TM2P-MISG-, and BTE-MISG-coated samples to CJ vapor (10.56 ± 0.96 ppm) were measured by absorption changes ΔA, given by:

$$\Delta A = A_{gas} - A_{air} \quad (3)$$

where A_{air} was the absorption in air, and A_{gas} was the absorption in the PVOC vapor. Both the CJ vapor generation and the sensing measurements were performed at room temperature.

Fig. 6a illustrated that no responses to CJ vapor were observed for NISG-modified LSPR sensors, which indicated that CJ absorption by the pure sol-gel matrix was poor, as reported previously [46]. The responses to CJ vapor for NISG/MISG-coated samples are summarized in Fig. 6b. MISGs without functional monomers exhibited lower responses than did the TMP-MISGs and TM2P-MISGs, indicating that the functional monomers improved the MISG responses and response speeds to target molecules. The TEP and BTE functional monomers had lower responses, indicating that functional monomers associated with $-OCH_2CH_3$ (TEP and BTE) were less effective in enhancing CJ imprinting than those containing $-OCH_3$ (TMP and TM2P). In addition, NISG-coated samples with the functional monomer TMP were studied. As shown in Fig. 6a, the affinity of NISGs to CJ vapor increased by adding TMP because of the TMP-NISG matrix effect. The response of TMP-MISGs was 2.25 times that of the TMP-NISGs. The larger sensitivity of the TMP-MISGs was attributed to both the matrix effect and imprinting. Therefore, TMP appeared to be the optimal functional monomer for the CJ-MISGs.

3.2. Optimization of the TBOT/TMP ratio

Imprinting with MIP materials was affected by the ratio of the matrix to the functional monomers [46]. Specifically, the ratios of matrix material (TBOT) to functional monomer (TMP) were adjusted to be 75/125, 100/100, 125/75, 150/50, and 175/25 (μL, v/v) to optimize the LSPR sensor for CJ detection. UV–vis absorption spectra vs. the ratios were plotted in Fig. 7, where A_{max}

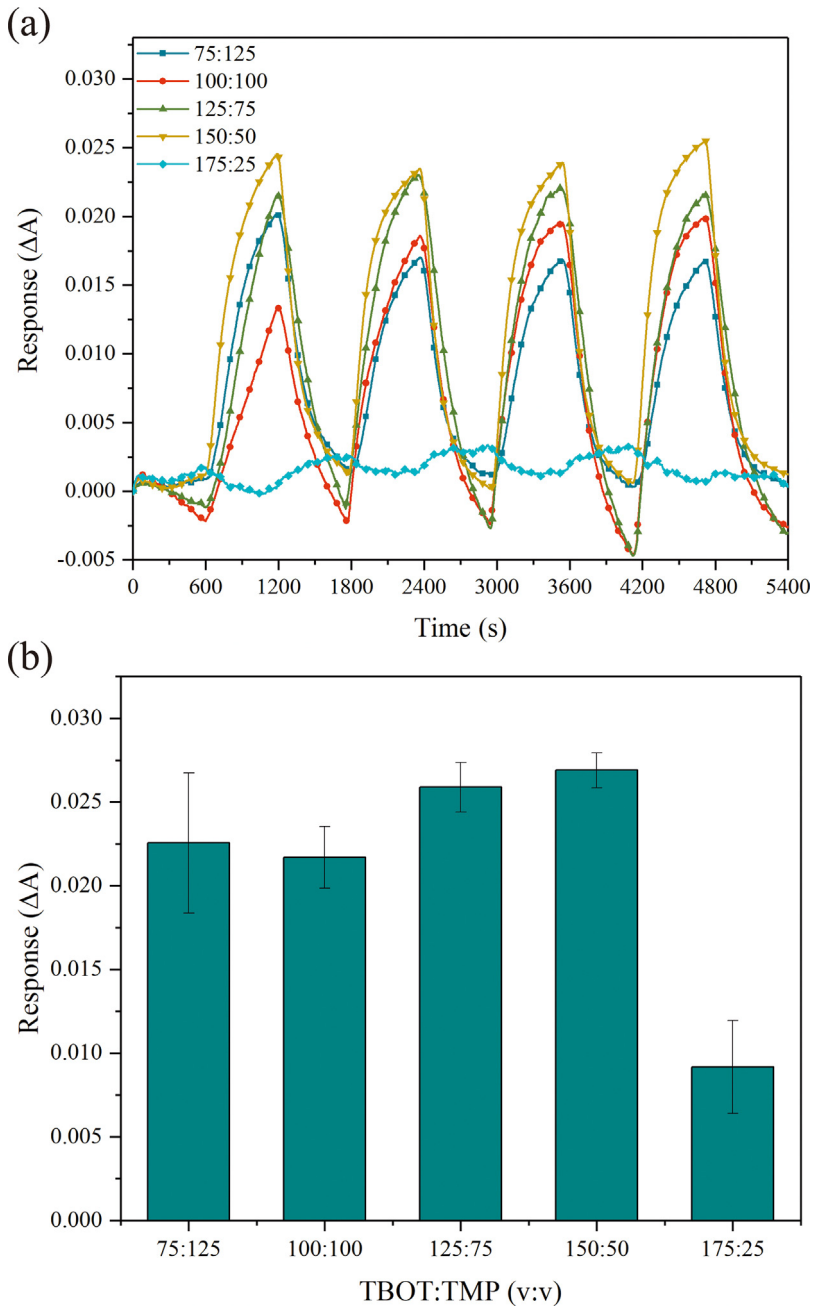

Fig. 8. Real-time responses of samples coated with TMP-MISG at TBOT/TMP = 75/125, 100/100, 125/75, 150/50, 175/25 (v/v) (a,) and their response summary (b). Responses were obtained for a CJ vapor flow for 600 s (10.56 ± 0.96 ppm), followed by an air flow for 600 s.

increased and its wavelength was blue-shifted as the amount of TMP decreased. SEM and AFM images for these MISGs (Figs. S3,4) revealed that the size of the TiO_2 sol-gel was affected by the ratios. In particular, larger TiO_2 discs were formed by a higher TBOT/TMP ratio.

In-situ responses of LSPR sensors coated with MISGs having the various TBOT/TMP ratios were plotted in Fig. 8. The results indicated that sensitivity was affected, and that Au nano-islands coated by MISG-TMP with the ratio TBOT/TMP = 150/50 had the highest CJ sensitivity.

3.3. CJ detection with a MISG-coated Au nano-island sensor

Both the shape and correct orientation of the functional groups enabled selective re-binding of the imprinted target by subsequent removal of the template binding sites during sol-gel processing. However, other PVOCs, specially terpene molecules, were present in the ambient environment and could be captured in MISG cavities. To evaluate the selectivity of the MISG-coated sensors, the three primary terpenes α-pinene, limonene, and γ-terpinene (Fig. 2) were tested as interference PVOCs. All the responses were normalized to these concentrations:

$$R_{normalized} = R/lg(C_{test}) \quad (4)$$

where R was the original LSPR sensor response. C_{test} was the testing concentration of each PVOC; specifically, 10.56 ± 0.96 ppm, 187.72 ± 33.64 ppm, 971.20 ± 58.89 ppm, and 750.05 ± 36.25 ppm for CJ, α-pinene, limonene and γ-terpinene vapors, respectively. The ratios of CJ to interference PVOCs (α-pinene, limonene and γ-terpinene) were calculated as 1:18, 1:92, 1:71, respectively.

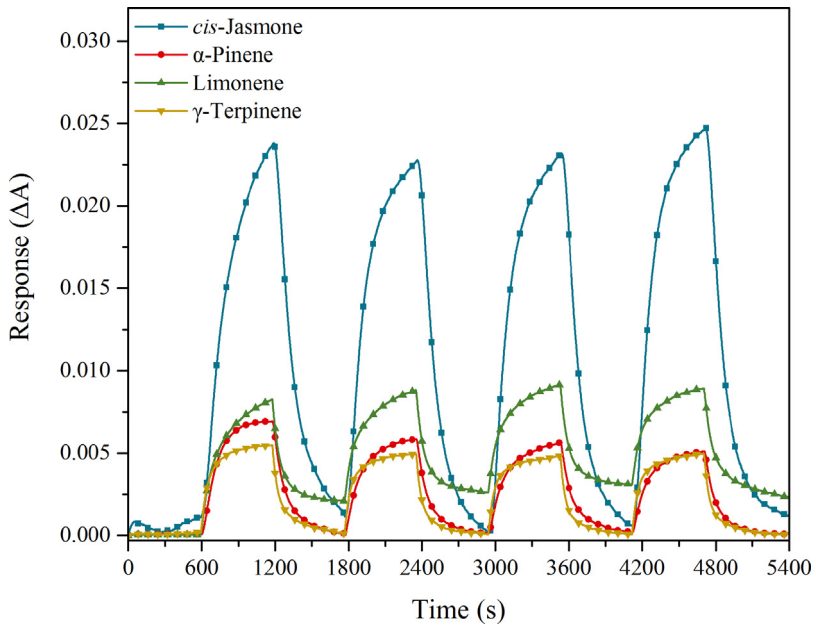

Fig. 9. Real-time responses of TMP-MISG-modified Au-islands to four types of PVOCs.

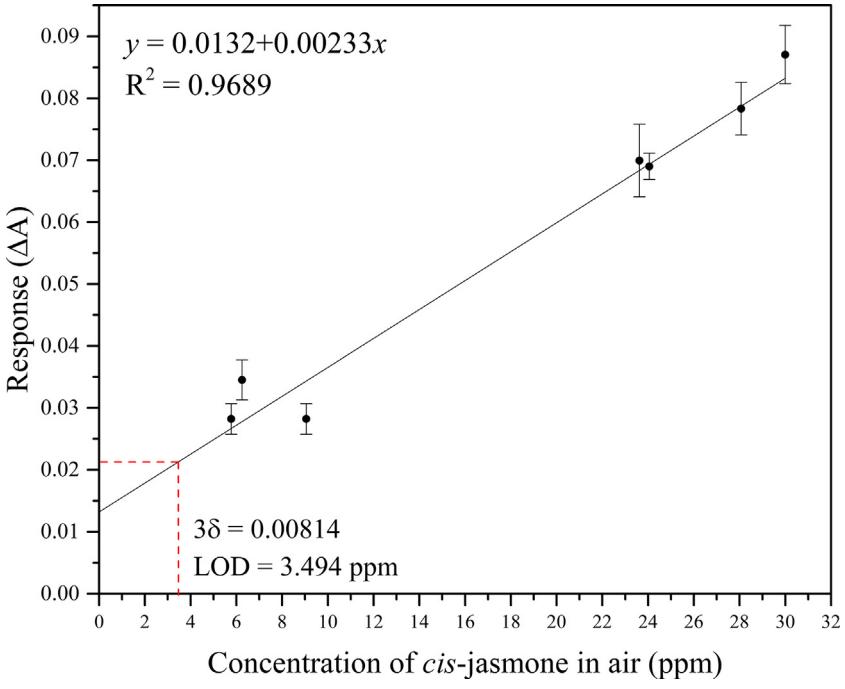

Fig. 10. Linear response vs. CJ concentration in air. The limit of CJ detection (LOD) was 3.5 ppm.

The normalized responses of the TMP-MISG-coated LSPR sensors to these interference PVOCs were plotted in Fig. 9. The CJ response of the molecularly imprinted sensor was much higher than that for the interfering molecules. This selectivity of the nanocomposite MISG-LSPR electrode was attributed to cavities that matched the shape and size of the CJ molecule. It has been reported that concentrations in agricultural environments of CJ, α-pinene, limonene, and γ-terpinene are about 85 ppm, 941 ppm, 171 ppm, and 371 ppm, respectively [47,48]. Therefore, the ratios of CJ to α-pinene, limonene, and γ-terpinene in agricultural environments can be calculated as 1:11, 1:2, and 1:4, respectively, which are larger than that in present study. It indicated that the sensor developed in present study would have enough selectivity in agricultural environments.

Quantitative CJ detection was performed by monitoring changes in the UV–vis absorption spectra for different CJ concentrations. A baseline signal was first collected in clean air. The LSPR sensors were then exposed to different CJ concentrations and the absorbances were obtained, as shown in Fig. 10. A linear calibration curve was fitted with:

$$y = 0.0132 + 0.00233x,\ R^2 = 0.9689;\ n = 3 \quad (5)$$

The limit of detection LOD = 3.494 ppm was calculated as the CJ concentration that resulted in a signal that was at least three times the baseline noise (3δ), where $m = 0.00233$ was the slope of the

calibration curve and δ was the standard deviation. Previous studies reported that CJ concentrations in shoots, leaves, and flowers were 0–85, 0–125 and 0–114 ppm, respectively [49–51]. Therefore, the sensor here would be sensitive enough for agricultural CJ detection.

Although a higher sensitivity could be obtained with additional functional monomers, the response intensity of the sensor was affected by the high concentrations of interfering molecules. Furthermore, when those concentrations were much higher than that of CJ, the of sensor response was unreliable. To overcome this problem, MISG-LSPR sensor arrays should be investigated for identification and detection of PVOCs in natural environments. By using different template molecule in the MISGs, a multi-channel sensing platform combined with pattern recognition methods could be tested.

4. Conclusions

LSPR sensors based on MISG-modified Au nano-islands was demonstrated for CJ vapor detection. The absorption of interference PVOCs (α-pinene, limonene and γ-terpinene) by $MISG_{cis\text{-jasmone}}$ were tested for CJ selectivity evaluation. The results demonstrated that sensor covered by MISGs with TMP had the strongest responses. In addition, the matrix to functional monomer ratio was optimized for better responsivity. Under optimal conditions, the volume ratio TBOT/TMP = 150/50 resulted in a 3.494-ppm LOD for CJ vapor. This was attributed to a porous imprinted composite film with CJ-selective binding sites. Real-time responses of the sensors displayed good selectivity, broad linearity, and repeatability. In conclusion, they are expected to provide sensitive PVOC detection for agricultural applications.

Acknowledgments

This research was supported by a grant from China Scholarship Council (CSC), JSPS KAKENHI Grant Number (15H01713) and Chongqing Postdoctoral Science Foundation under Grant numbers Xm2017101.

Appendix A. Supplementary data

Supplementary data associated with this article can be found, in the online version, at https://doi.org/10.1016/j.snb.2017.12.123.

References

[1] C. Di, C. Ning, L.Q. Huang, C.Z. Wang, Design of larval chemical attractants based on odorant response spectra of odorant receptors in the cotton bollworm, Insect Biochem. Mol. Biol. 84 (2017) 48–62.
[2] J.P. da Graca, T.E. Ueda, T. Janegitz, S.S. Vieira, M.C. Salvador, M.C.N. de Oliveira, et al., The natural plant stress elicitor cis-jasmone causes cultivar-dependent reduction in growth of the stink bug, Euschistus heros and associated changes in flavonoid concentrations in soybean Glycine max, Phytochemistry 131 (2016) 84–91.
[3] E.L. Wason, A.A. Agrawal, M.D. Hunter, A genetically-based latitudinal cline in the emission of herbivore-induced plant volatile organic compounds, J. Chem. Ecol. 39 (2013) 1101–1111.
[4] S. Tamogami, K. Noge, M. Abe, G.K. Agrawal, R. Rakwal, Deuterium labeling for investigating de novo synthesis of terpene volatiles in Achyranthes bidentata, Biotechnol. Lett. 35 (2013) 1247–1252.
[5] S. Tamogami, R. Ralkwal, G.K. Agrawal, Interplant communication: airborne methyl jasmonate is essentially converted into JA and JS-Ile activating jasmonate signaling pathway and VOCs emission, Biochem. Biophys. Res. Commun. 376 (2008) 723–727.
[6] I.S. Sobhy, C.M. Woodcock, S.J. Powers, J.C. Caulfield, J.A. Pickett, M.A. Birkett, Cis-jasmone elicits aphid-induced stress signalling in potatoes, J. Chem. Ecol. 43 (2017) 39–52.
[7] M.A. Birkett, C.A.M. Campbell, K. Chamberlain, E. Guerrieri, A.J. Hick, J.L. Martin, et al., New roles for cis-jasmone as an insect semiochemical and in plant defense, Proc. Natl. Acad. Sci. U. S. A. 97 (2000) 9329–9334.
[8] G. Buchi, H. Wuest, An efficient synthesis of cis-jasmone, J. Org. Chem. 31 (1966) 977–978.
[9] M. Stitz, K. Gase, I.T. Baldwin, E. Gaquerel, Ectopic expression of atjmt in nicotiana attenuata: creating a metabolic sink has tissue-specific consequences for the jasmonate metabolic network and silences downstream gene expression, Plant Physiol. 157 (2011) 341–354.
[10] C.C. von Dahl, I.T. Baldwin, Methyl jasmonate and cis-jasmone do not dispose of the herbivore-induced jasmonate burst in nicotiana attenuata, Physiol. Plant. 120 (2004) 474–481.
[11] D.M. Mutyambai, T.J.A. Bruce, J. van den Berg, C.A.O. Midega, J.A. Pickett, Z.R. Khan, An indirect defence trait mediated through egg-induced maize volatiles from neighbouring plants, PLoS One 11 (2016).
[12] Z.X. Han, M.M. Rana, G.F. Liu, M.J. Gao, D.X. Li, F.G. Wu, et al., Green tea flavour determinants and their changes over manufacturing processes, Food Chem. 212 (2016) 739–748.
[13] M. Delgado-Rodriguez, M. Ruiz-Montoya, I. Giraldez, R. Lopez, E. Madejon, M.J. Diaz, Use of electronic nose and GC–MS in detection and monitoring some VOC, Atmos. Environ. 51 (2012) 278–285.
[14] N. Alipour, R.L. Andersson, R.T. Olsson, U.W. Gedde, M.S. Hedenqvist, Voc-induced flexing of single and multilayer polyethylene films as gas sensors, ACS Appl. Mater. Inter. 8 (2016) 9946–9953.
[15] A. Caron, N. Redon, F. Thevenet, B. Hanoune, P. Coddeville, Performances and limitations of electronic gas sensors to investigate an indoor air quality event, Build. Environ. 107 (2016) 19–28.
[16] J.H. Lee, H.G. Byun, Chemosensors and Chemoreception, Anal. Bioanal. Chem. 406 (2014) 3929.
[17] O. Adegoke, M. Morita, T. Kato, M. Ito, T. Suzuki, E.Y. Park, Localized surface plasmon resonance-mediated fluorescence signals in plasmonic nanoparticle-quantum dot hybrids for ultrasensitive zika virus RNA detection via hairpin hybridization assays, Biosens. Bioelectron. 94 (2017) 513–522.
[18] E. Mauriz, A. Calle, J.J. Manclus, A. Montoya, A. Hildebrandt, D. Barcelo, et al., Optical immunosensor for fast and sensitive detection of DDT and related compounds in river water samples, Biosens. Bioelectron. 22 (2007) 1410–1418.
[19] D.R. Shankaran, K.V. Gobi, T. Sakai, K. Matsumoto, K. Toko, N. Miura, Surface plasmon resonance immunosensor for highly sensitive detection of 2,4,6-trinitrotoluene, Biosens. Bioelectron. 20 (2005) 1750–1756.
[20] D.S. Boyuk, L.W. Chou, M.A. Filler, Strong near-field coupling of plasmonic resonators embedded in Si nanowires, ACS Photonics 3 (2016) 184–189.
[21] C.C. Evans, C.Y. Liu, J. Suntivich, Tio2 nanophotonic sensors for efficient integrated evanescent Raman spectroscopy, ACS Photonics 3 (2016) 1662–1669.
[22] C.H. Fang, G.L. Zhao, Y.L. Xiao, J. Zhao, Z.J. Zhang, B.Y. Geng, Facile growth of high-yield gold nanobipyramids induced by chloroplatinic acid for high refractive index sensing properties, Sci. Rep. 6 (2016).
[23] M.S. Kirschner, C.M. Lethiec, X.M. Lin, G.C. Schatz, L.X. Chen, R.D. Schaller, Size-dependent coherent-phonon plasmon modulation and deformation characterization in gold bipyramids and nanojavelins, ACS Photonics 3 (2016) 758–763.
[24] K.Q. Lin, J. Yi, S. Hu, J.J. Sun, J.T. Zheng, X. Wang, et al., Intraband hot-electron photoluminescence from single silver nanorods, ACS Photonics 3 (2016) 1248–1255.
[25] J.R.L. Guerreiro, N. Teixeira, V. De Freitas, M.G.F. Sales, D.S. Sutherland, A saliva molecular imprinted localized surface plasmon resonance biosensor for wine astringency estimation, Food Chem. 233 (2017) 457–466.
[26] S. Kamimura, S. Yamashita, S. Abe, T. Tsubota, T. Ohno, Effect of core@shell (Au@Ag) nanostructure on surface plasmon-induced photocatalytic activity under visible light irradiation, Appl. Catal. B 211 (2017) 11–17.
[27] A.V. Skinner, S. Han, R. Balasubramanian, Rapid selective colorimetric sensing of polyphosphates by ionic resorcinarene cavitand interdigitated gold nanoparticles, Sens. Actuators B 247 (2017) 706–712.
[28] A. Thakur, G.Y. Qiu, N.G. Siu-Pang, J.T. Guan, J.B. Yue, Y.J. Lee, et al., Direct detection of two different tumor-derived extracellular vesicles by SAM-AuNIs LSPR biosensor, Biosens. Bioelectron. 94 (2017) 400–407.
[29] Y.C. Wang, L. Lu, S. Gunasekaran, Biopolymer/gold nanoparticles composite plasmonic thermal history indicator to monitor quality and safety of perishable bioproducts, Biosens. Bioelectron. 92 (2017) 109–116.
[30] J.M. Lim, N.S. Heo, S.Y. Oh, M.Y. Ryu, J.H. Seo, T.J. Park, et al., Selection of affinity peptides for interference-free detection of cholera toxin, Biosens. Bioelectron. 99 (2018) 289–295.
[31] A. Urrutia, J. Goicoechea, P.J. Rivero, A. Pildain, F.J. Arregui, Optical fiber sensors based on gold nanorods embedded in polymeric thin films, Sens. Actuators B 255 (2018) 2105–2112.
[32] M.D. Allendorf, R.J.T. Houk, L. Andruszkiewicz, A.A. Talin, J. Pikarsky, A. Choudhury, et al., Stress-induced chemical detection using flexible metal-organic frameworks, JACS 130 (2008) 14404–+.
[33] V.T. Tran, H.J. Zhou, S. Kim, J. Lee, J. Kim, F.M. Zou, et al., Self-assembled magnetoplasmonic nanochain for DNA sensing, Sens. Actuators B 203 (2014) 817–823.
[34] B. Chen, C.J. Liu, L.P. Ge, K. Hayashi, Localized surface plasmon resonance gas sensor of Au nano-islands coated with molecularly imprinted polymer: influence of polymer thickness on sensitivity and selectivity, Sens. Actuators B 231 (2016) 787–792.
[35] K. Qian, Q.L. Deng, G.Z. Fang, J.P. Wang, M.F. Pan, S. Wang, et al., Metal-organic frameworks supported surface-imprinted nanoparticles for the sensitive detection of metolcarb, Biosens. Bioelectron. 79 (2016) 359–363.
[36] B. Rezaei, M.K.L. Boroujeni, A.A. Ensafi, Caffeine electrochemical sensor using imprinted film as recognition element based on polypyrrole, sol-gel, and gold

nanoparticles hybrid nanocomposite modified pencil graphite electrode, Biosens. Bioelectron. 60 (2014) 77–83.
[37] K. Haupt, K. Mosbach, Molecularly imprinted polymers and their use in biomimetic sensors, Chem. Rev. 100 (2000) 2495–2504.
[38] E.L. Holthoff, F.V. Bright, Molecularly imprinted xerogels as platforms for sensing, Acc. Chem. Res. 40 (2007) 756–767.
[39] Y.J. Tong, H.D. Li, H.M. Guan, J.M. Zhao, S. Majeed, S. Anjum, et al., Electrochemical cholesterol sensor based on carbon nanotube@molecularly imprinted polymer modified ceramic carbon electrode, Biosens. Bioelectron. 47 (2013) 553–558.
[40] L. Shang, C.J. Liu, M. Watanabe, B. Chen, K. Hayashi, LSPR sensor array based on molecularly imprinted sol-gels for pattern recognition of volatile organic acids, Sens. Actuators B 249 (2017) 14–21.
[41] B. Chen, C.J. Liu, K. Hayashi, Selective terpene vapor detection using molecularly imprinted polymer coated Au nanoparticle LSPR sensor, IEEE Sens. J. 14 (2014) 3458–3464.
[42] K. Wang, X.W. Guan, S.G. Chai, Q.C. Zou, X.H. Zhang, J.Z. Zhang, A novel, molecularly imprinted polymer sensor made using an oligomeric methyl silsesquioxane-TiO2 composite sol on a glassy carbon electrode for the detection of procainamide hydrochloride, Biosens. Bioelectron. 64 (2015) 94–101.
[43] W.A. Braunecker, K. Matyjaszewski, Controlled/living radical polymerization: features, developments, and perspectives, Prog. Polym. Sci. 32 (2007) 93–146.
[44] V. Percec, T. Guliashvili, J.S. Ladislaw, A. Wistrand, A. Stjerndahl, M.J. Sienkowska, et al., Ultrafast synthesis of ultrahigh molar mass polymers by metal-catalyzed living radical polymerization of acrylates, methacrylates, and vinyl chloride mediated by SET at 25 °C, JACS 128 (2006) 14156–14165.
[45] B. Chen, M. Mokume, C.J. Liu, K. Hayashi, Structure and localized surface plasmon tuning of sputtered Au nano-islands through thermal annealing, Vacuum 110 (2014) 94–101.
[46] C.J. Liu, B. Wyszynski, R. Yatabe, K. Hayashi, K. Toko, Molecularly imprinted sol-gel-based QCM sensor arrays for the detection and recognition of volatile aldehydes, Sensors 17 (2017).
[47] H.N. Nigg, D. Seigler, Phytochemical Resources for Medicine and Agriculture, Springer Science & Business Media, 2013.
[48] B. Bussell, J. Considine, Z. Spadek, Flower and volatile oil ontogeny in boronia megastigma, Ann. Bot. 76 (1995) 457–463.
[49] J.A. Duke, Handbook of Phytochemical Constituent Grass, Herbs and Other Economic Plants, CRC press, 1992.
[50] W.S. Schlotzhauer, S.D. Pair, R.J. Horvat, Volatile constituents from the flowers of japanese honeysuckle (lonicera japonica), J. Agric. Food Chem. 44 (1996) 206–209.
[51] K. Tatsuka, S. Suekane, Y. Sakai, H. Sumitani, Volatile constituents of kiwi fruit flowers-simultaneous distillation and extraction versus headspace sampling, J. Agric. Food Chem. 38 (1990) 2176–2180.

Biographies

Liang Shang received the B.S. degree in mechanical manufacturing and automation and the M.S. degree in agricultural mechanization engineering from Northwest A&F University, Shannxi, China, in 2012 and 2015, respectively. He is currently pursuing the Ph.D. degree at Kyushu University, Fukuoka, Japan, and engaging in research related to gas and odor sensors.

Chuanjun Liu received his PhD degree in material engineering from Nagaoka University of Technology (Japan) in 2006. He has worked as research fellow in Nagaoka University of Technology (from 2006) and Kyushu University (from 2008), and as assistant professor at the Graduate School of Information Science and Electrical Engineering of Kyushu University (from 2012) and associate professor of R&D center for Taste and Odor Sensing (TAOS) of Kyushu University (from 2016). He is now a principle researcher in Research Laboratory of U.S.E. Co. LTD, Japan. He is a member of the Society of Polymer Science Japan and the Institute of Electrical Engineers of Japan. His research interests include the development and application of organic electronic devices, nanoscale sensing materials, and gas and odor sensors.

Bin Chen received her PhD degree in the Graduate School of Information Science and Electrical Engineering from Kyushu University (Japan) in 2014. She is now a lecturer at the College of Electronic and Information Engineering at Southwest University, and engaging in the research of chemical sensors.

Kenshi Hayashi received his BE, ME, and PhD degree, all in electrical engineering, from Kyushu University (Japan) in 1982, 1984, and 1990, respectively. He is now a professor at the Graduate School of Information Science and Electrical Engineering of Kyushu University. He is a member of the Japan Society of Applied Physics and the Institute of Electrical Engineers of Japan. His research interests include: information service using odor cluster matching, visualization of odor space, measurement and coding of odor quality and quantity, novel devices using molecular wire and organic electronic material, and biometrics by odor sensing.